POLITECNICO MILANO 1863

EXECUTIVE SUMMARY OF THE THESIS

Experimental study on the flow boiling critical heat flux of narrow channels heat sinks for power electronics

TESI MAGISTRALE IN ENERGY ENGINEERING – INGEGNERIA ENERGETICA

AUTHOR: HUGO ALEJANDRO POZO SARAVIA

ADVISOR: LUIGI PIETRO MARIA COLOMBO

ACADEMIC YEAR: 2020-2021

1. Introduction

The growing importance of sustainable cooling systems in modern microelectronics presents flow-boiling in microchannels as a long-term solution with great potential to meet the current targets, i.e., of 250 W/cm^2 [1] at the chip level for electric vehicles with minimum pressure losses. The maximum achievable heat flux is generally referred to as the critical heat flux (CHF). Surpassing the CHF commonly results in a sharp increase of the heated surface temperature and may lead to a physical burnout of the electronics making it the most relevant limit in the design of microelectronics power systems. Compared to the conventional single-phase cooling systems, flow boiling in microchannels presents three main advantages: (1) the latent heat of vaporization leading to very high heat transfer during boiling, (2) the large surface area to volume ratio of microchannel geometries, and (3) smaller flow rate and more uniform wall temperature [2,6]. Two-phase instabilities in microchannels might trigger earlier CHF, and they are generally more pronounced at lower mass fluxes and low subcooling. The current study strives to achieve a high CHF based on the footprint area with a minimal pressure drop. The investigations concerning saturated CHF in multi-microchannels aligned with the scope of the thesis are summarized in Table 1. The operational conditions cover a large range of saturation temperatures, mass fluxes, inlet subcooling, and heated equivalent diameters. The past investigations in Table 1 did not always attempt to achieve high CHF, as pointed out by Park and Thome [6], nonetheless, it is important to mention that the maximum footprint CHF in these studies is only partly covering current targets for power electronics in electric vehicles [1].

Abbreviations: CHF, critical heat flux; GWP, global warming potential; MAE, mean average error; RTD, resistance thermal detector.

1.1. Effect of parameters

The CHF in microchannels is affected by several parameters regarding the channel geometry and fluid conditions. Previous investigations indicate that the increase of mass flux consistently increases the CHF. However, some inconsistencies are found in the subcooling effect. The CHF either increases or is unaffected by the level of inlet subcooling. Park and Thome [6] attributed the independence of inlet subcooling to their longer heated length. Later, Mauro et al. [2] using the same test samples and a split system found an increasing effect with subcooling. In a recent study by Kærn et al. [3] using inlet restriction to stabilize the flow, the subcooling effect on the CHF was evident, especially at large mass fluxes. In general, previous investigations suggest that the inlet subcooling effect on the CHF is highly related to the flow instabilities in multi-channels, the heated length, and the fluid.

Similarly, some inconsistencies are found in the literature concerning the effects of saturation temperature on the CHF. The increase in saturation

Table 1. Main parameters, conditions, and effects observed in multi-microchannel saturated CHF studies

Author	Geometry				Fluids	Conditions				Effects
	$N \times (W_{ch} \times H_{ch})$ [μm]	L_h [mm]	D_{he} [μm]	H_{ch}/W_{ch} [−]		T_{sat}	G	ΔT_{sub}	q''^{max}_{fp}	
Park, Thome [6]	29 x (199 x 756)	20	56	3.8	R134a	15-40	200-4000	0-15	215	CHF↑ with G CHF → with ΔT_{sc} and T_{sat}
Mauro et al. [2]	29 x (199 x 756)	10	28	3.8	R245fa, R236fa, R134a	15-40	250-1500	5-25	330	CHF↑ with G and ΔT_{sc} CHF↓ with T_{sat}
Kærn et al. [3]	25 x (198 x 1167)	10	365	5.89	R134a, R1234yf,	30-40	333-1260	(1.3-	678	CHF↑ with G, ΔT_{sc}
	17 x (293 x 1176)	10	521	4.01	R1234ze(E)			14.7)		CHF↓ with T_{sat}
Fu et al. [4]	6 x (300 x 300)	20	400	0.45	HFE-7100	61	39-180		114	CHF↑ with G
	6 x (300 x 4000)	20	1120	6.06						CHF↑ with *diverging*
Xia et al. [5]	16 x (128 x 80)	120	98	0.626	Acetone	56	251-423	26	601	CHF↑ with G CHF↑ with *wavy*

Nomenclature

Roman letters

A	area, m^2
D_{wet}	wetted diameter, $4A_{ch}/P_{wet}$, m.
D_{he}	heated equivalent diameter, $4A_{ch}/P_h$, m
G	mass flux, kg/m^2s
h	specific enthalpy, J/kg
h_{tc}	heat transfer coefficient, W/m^2K
H	height, m
I	current, A
k	thermal conductivity, W/mK
L	length, m
N	number of channels, −
p	pressure, bar
P_{wet}	wetted perimeter, $W_{ch} + 2\eta H_{ch}$, m
P_h	heated equivalent perimeter, $W_{ch} + 2H_{ch}$, m
q	heat flux
t	thickness, m
T	temperature, ℃
V	voltage, V
W	width, m
x	vapor quality, −

Greek letters

η	Fin efficiency, −
μ	Viscosity, Pa s
ρ	Density, kg/m^3
σ	Surface tension, N/m

Subscripts

ch	channel
cr	critical
l	liquid
f	fin
fp	footprint
v	vapor
sat	saturation
sub	subcooling
w	wall

temperature could either increase or decrease the CHF depending on the fluid and the reduced pressure. Park and Thome [6] found increasing and decreasing trends for their larger diameter channels. Mauro [2] found that the saturation effect decreased the CHF with R134a and R236fa, but it was unaffected with R245fa. The increasing and decreasing trend is commonly explained by the counteracting effects of the increased vapor to liquid density ratio ρ_v/ρ_l and the latent heat of vaporization Δh_{vl} and the surface tension σ decrease [3], suggesting the existence of a peak CHF. Concerning the geometric parameters, it is difficult to make a direct comparison regarding the CHF in multi-channels since most studies involve only a single test sample, and the wall thickness and channel number employed varies among different authors.

In addition, comparative investigations of different wall geometry are scarce and the effect of new heat sink designs on CHF is not established. Alternatives to the conventional straight channels, such as diverging designs indicated a promising reduction of flow instability in microchannels, hence increasing the CHF. A study by Fu et al. [4] demonstrated that the CHF was higher with their diverging channels compared to the conventional straight ones, especially at low mass fluxes while the pressure drop was significantly reduced. Another alternative to the conventional straight microchannels is the sinusoidal wavy design, however, flow boiling heat transfer studies are particularly limited. In a recent study, Xia et al. [5] obtained a significantly higher CHF with their test samples, reaching values of 601 W/cm^2 with wavy walls. The above findings suggest that the CHF can be enhanced with different wall geometry.

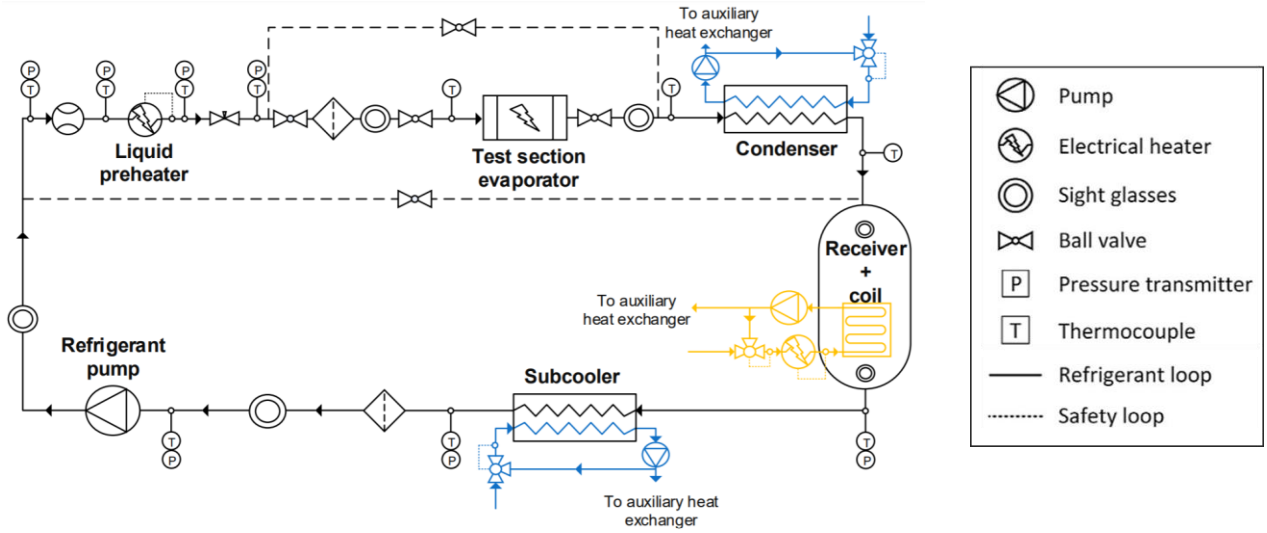

Fig. 1. Schematic diagram of the experimental flow boiling test facility.

1.2. Purpose, hypothesis, and objectives

The present thesis aims to achieve a higher footprint CHF and contribute to the general discussion on the effects of the main parameters of interest in flow boiling by using saturated flow boiling of refrigerants in narrow high aspect ratio microchannels with thin separating walls, and different wall geometries. The investigation hypothesizes that flow boiling in narrow channels could achieve high CHF, and alternative wall geometries could enhance the CHF or decrease significantly the pressure drop. The novelty of the present study consisted in performing a comparative analysis of the CHF effect by different wall geometries, such as diverging and sinusoidal wavy channel designs, to the conventional straight channels. The objectives of the study are formulated as follows: the first objective was to document an improvement of footprint CHF, the second objective was to investigate the effects of the main parameters on the CHF, and the third objective was to evaluate the applicability of existing CHF correlations in the investigated narrow and high aspect ratio channels with low-GWP refrigerants.

2. Experimental Methods

2.1. The refrigerant loop

The refrigerant loop consists of the components to regulate the saturation temperature in the test section, the mass flux in the channels, and the inlet sub-cooling. Fig. 1 presents a schematic of the flow conditioning loop of the experimental test facility. The refrigerant is accumulated in the cylindrical receiver and sent through a plate heat exchanger (sub-cooler) until a slight level of subcooling is obtained. Afterward, the liquid refrigerant pressure is increased through a gear pump, and later, it is balanced with a needle valve. Finally, the liquid pre-heater raises the temperature of the refrigerant before entering the test section. After boiling occurs in the test section, the two-phase flow is condensed in the second heat plate exchanger (condenser) and collected back to the receiver. All signals were collected by data acquisition modules, and the temperature set-points and the heating power supply were monitored and controlled in a customized Labview interface. The control and regulation of the mass flux were done by manually adjusting the motor speed of the pump using a variable frequency speed drive. The desired level of inlet subcooling was controlled by regulating the liquid pre-heater power supply. Finally, the saturation pressure was controlled by the receiver temperature.

2.2. Test section

Fig. 2 presents a schematic view of the exploded view of the main components of the test section where the measurements of interest are obtained. The section was designed to facilitate the interchange between heat sinks. In the current investigation, three test samples with different wall geometries were employed: geometry *C* with straight channels, geometry *H* with diverging channels, and geometry *G* with sinusoidal wavy channels. The detail of the dimensions is presented in Table 2.

The additional components of the test section are the microheater, the steel chassis, and the top cover. The microheater was manufactured to allow infrared temperature measurements and to mirror a real po-

Table 2. Channel dimensions for geometry C, H, and G.

Geometry	W_{ch} [μm]	H_{ch} [μm]	W_{fin} [μm]	D_h [μm]	N [−]
C ($straigth$)	198	1167	200	338	25
H ($diverging$)	200 − 340*	1200	200 − 60*	343	25
G ($wavy$)	200	1200	200	338	25

* Indicates that the values correspond to the inlet and outlet of the channels.

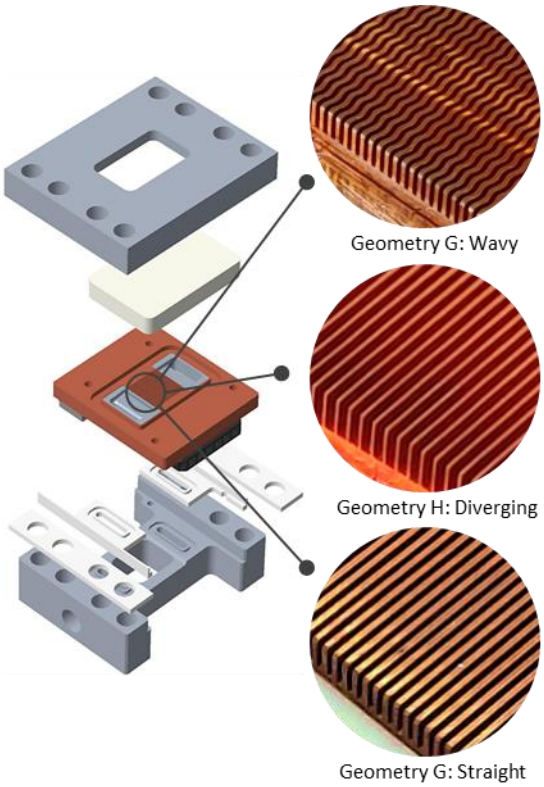

Fig. 2. Exploded view of the test section CAF model.

wer electronics application. It consists of a 0.88 µm thick platinum serpentine on a 350 µm silicon wafer. Additionally, four 4-wire platinum resistance thermal detectors (RTDs) are placed at the serpentine heater. The top cover consists of a stainless-steel structure with a central cavity and borosilicate glass and allows visual access to the high-speed camera.

2.1. CHF detection

The CHF detection was performed by gradually increasing the voltage of the power supply until a sharp increase in the RTDs occurred. In the case of being far away from the CHF, the signal of the RTDs resulted in an increment of first-order response. However, when the CHF occurred, the RTDs presented a second-order order growth which triggered the safe stop of the setup cutting the power supply. In this case, the power supply was reduced by 0.25 V and the measurement of a point was obtained once the steady-state of the system was verified. The steady-state condition was defined by observing a temperature variation of fewer than 0.05 °C over a 120 s interval.

2.4. Data reduction

The heat flux at the footprint level of the channels was calculated considering the heat loss, according to the equation:

$$q_{fp} = \frac{V.I - \dot{Q}_{AMB}}{A_{fp}} \quad (1)$$

where A_{fp} is the total footprint area of the heat sink, V is the voltage of the power supply, and I is current of the microheater. The heat losses $\dot{Q}_{AMB}$ from the test section was determined on a separate test with single-phase measurements.

The heat flux at the wall of the channels was calculated by the adiabatic tip fin model. The fin efficiency and fin parameter for the diverging channels were calculated considering the effect of the thickness reduction of the wall at the outlet section, while the effect of corrugations was ignored for the wavy channels and the walls were treated as if they were straight by employing an area enlargement factor Φ. The resulting equations are:

$$q_W = \frac{q_{fp}\left(W_f + W_{ch}\right)}{\left(W_{ch} + 2\eta H_{ch}\right)} \quad (2)$$

$$m = \sqrt{\frac{h_{tc}\, 2\left(W_f + L_{ch}\right)}{k_{Cu} W_f L_{ch}}} \quad (3)$$

$$\eta = \frac{\tanh(mH_{ch})}{mH_{ch}} \quad (4)$$

where k_{Cu} is the thermal conductivity of copper, m is the fin parameter, and η is the fin efficiency. The heat transfer coefficient h_{tc} was calculated by

$$h_{tc} = \frac{q_w}{T_W - T_{sat}} \quad (5)$$

where the temperature at the wall T_w was calculated assuming 1-D conduction through the solder, silicon layer, and the copper of the heat sink, resulting in:

$$T_W = T_h - \Delta T_{Si} - \Delta T_{Sn} - \Delta T_{Cu} \quad (6)$$

$$\Delta T_j = k_j\, q_{fp}/t_j \qquad j \in \{Si, Sn, Cu\} \quad (7)$$

where the temperature of the heater T_h was obtained by the average of the RTDs. The critical (outlet) vapor quality was calculated by energy balance resulting in the equation:

$$x_{cr} = \frac{q_w}{G.\Delta h_{fg}} . \frac{P_{wet}}{A_{ch}} - \frac{\Delta h_{sub}}{\Delta h_{fg}} \quad (8)$$

$$= \frac{q_w}{G.\Delta h_{fg}} . \frac{4.L_h}{D_{wet}} - \frac{\Delta h_{sub}}{\Delta h_{fg}} \quad (9)$$

The critical vapor quality can reveal the definition of the hydraulic diameter using the effective wetted perimeter P_{wet}. This later can be used to expose the effective wetted perimeter D_{wet}, as shown in equation 9.

2.5. Experimental uncertainty

The single sample error propagation method by Kline and McClintock [7] was employed to calculate the experimental uncertainties risen from the data reduction, where no correlation between the input variables was assumed. The uncertainties were well accepted for the study.

2.5. Experimental design

The investigation adopted a low-GWP fluid (R1234yf) and the conventional R134a. Three different microchannels test samples were manufactured in copper and the measurements resulted in a large data bank with 216 data points taken under a wide range of mass flux between 320 kg/m^{2}s to 1200 kg/m^{2}s, at different subcooling, and a saturation temperature of 30 °C and 40 °C. An infrared camera with a resolution of 221 x 221 pixels was used, and high-speed visualization was employed to support the investigation with flow pattern analysis and verify the absence of relevant flow instabilities.

3. Results

3.1. Footprint CHF

Fig. 3 presents the footprint CHF results versus mass flux with R134a at different inlet subcooling for a nominal saturation temperature of 30 °C. Fig. 4 shows the same results with R1234yf. The footprint CHF increased with increasing mass flux in all test conditions according to the literature, and in all test conditions, CHF was found to decrease with R1234yf. The region of low mass flux is characterized by a steep increase in the CHF, while at high mass it presents a flattening pattern. The highest CHF is obtained with geometry G and with R134a at a saturation temperature of 30 °C, resulting in a value of 852.1 W/cm^2 at the highest mass flux, which is notoriously higher than previous investigations, while geometry H and geometry C present similar results. Fig. 5 presents the ratio between the CHF at saturation of 30 °C and saturation of 40 °C with R1234yf. The CHF consistently decreased when increasing the saturation temperature from 30 °C to 40 °C, but in all cases, the reduction is no more than 10%. This could be attributed to the reduction in the surface tension and the heat of vaporization that decrease with increased saturation temperature.

Fig 6a-c presents the footprint CHF versus the inlet subcooling at a saturation temperature of 40 °C with R134a. The effect of inlet subcooling on the footprint

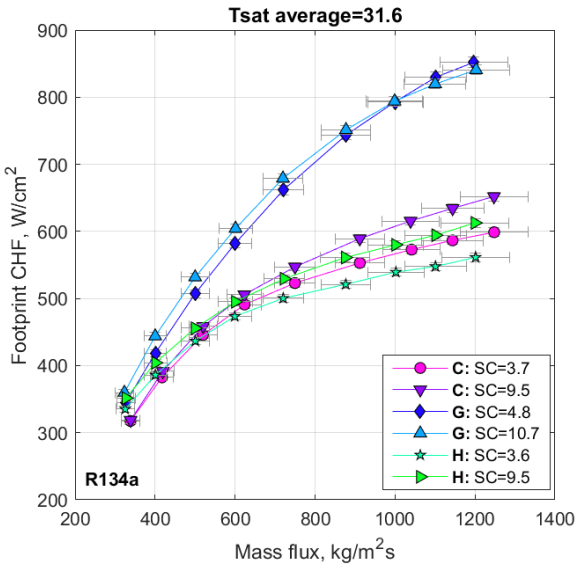

Fig. 3. Footprint CHF vs. mass flux for R134a at an average saturation temperature of 31.6 °C and different subcooling (SC).

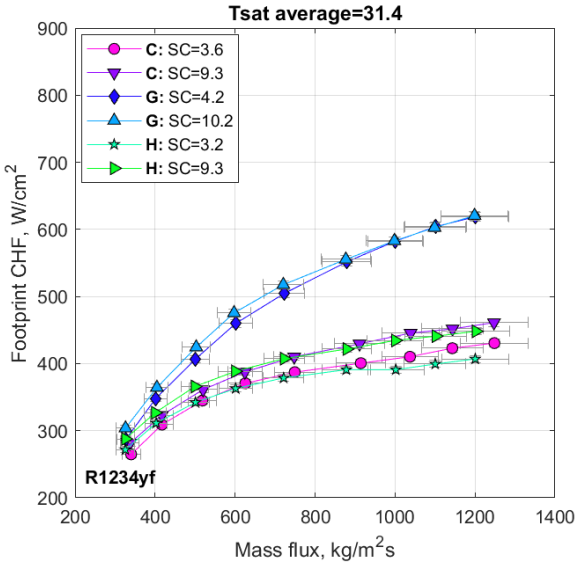

Fig. 4. Footprint CHF vs. mass flux for R1234yf at an average saturation temperature of 31.4 °C and different subcooling (SC).

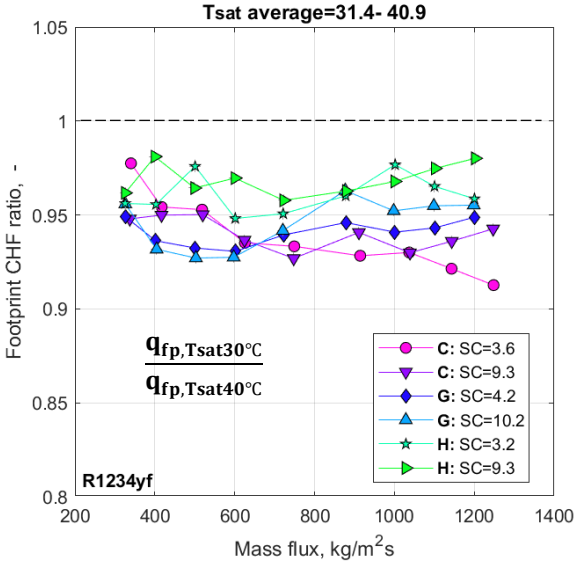

Fig. 5. Footprint CHF ratio of saturation of 30 °C and 40 °C.

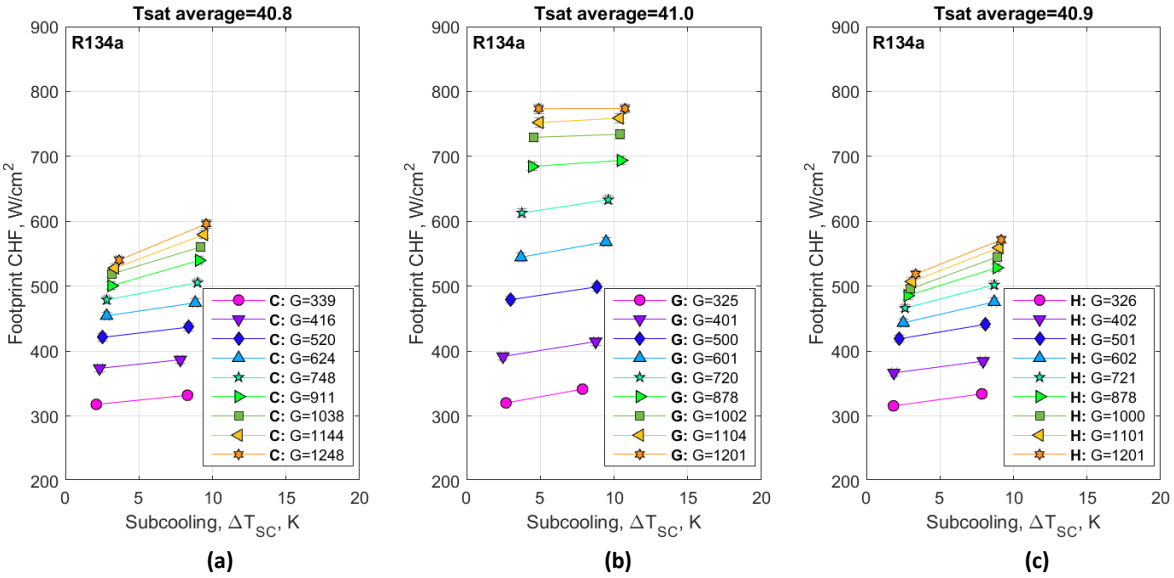

Fig. 6. Footprint CHF vs. inlet subcooling for R134a at nominal saturation temperature of 40°C (a) for geometry C, (b) G, (c), and H.

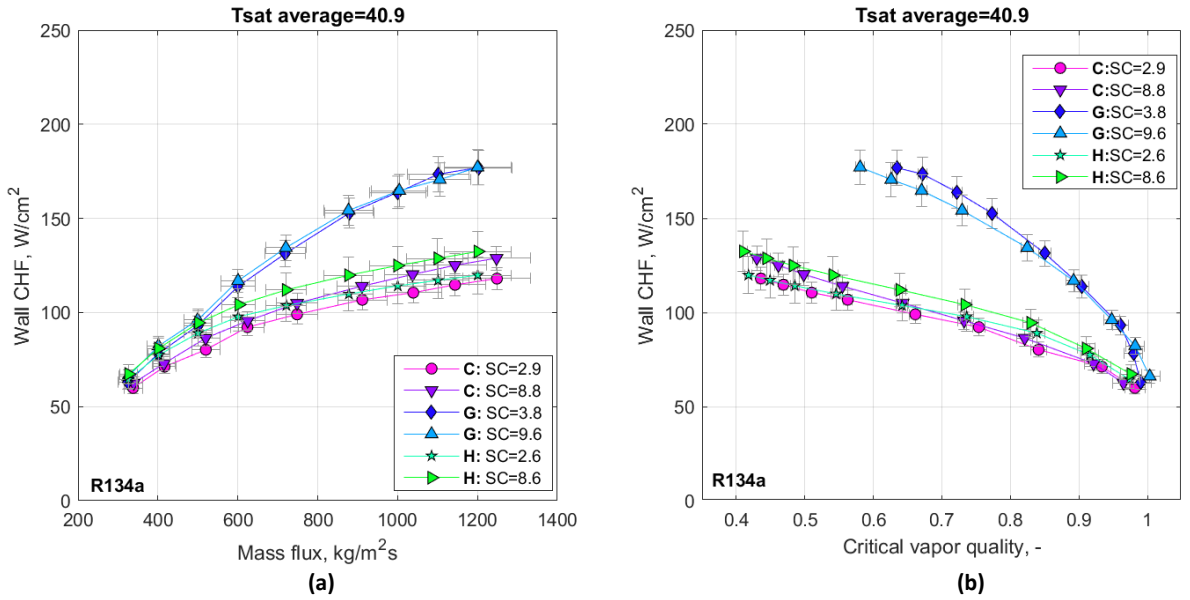

Fig. 7. (a) Wall CHF vs. mass flux and (b) wall CHF vs. critical vapor quality for R134a at an average saturation temperature of 40.9 °C.

CHF with geometry H and C is evident, especially at high mass flux. Interestingly, the opposite trend is found with geometry G where the footprint CHF increases with inlet subcooling in the low-mass-flux region, while it is unaffected at high mass flux. The reverse tendencies can be attributed to the high mixing and secondary flows in the corrugated walls of geometry G that quickly raise the temperature of the incoming liquid to the saturation one, thus eliminating the subcooling effect, especially at higher mass velocities.

3.2. Wall CHF

Fig.7a presents the CHF at the channel walls versus the mass flux for nominal saturation temperatures of 30 °C and 40 °C with R134a. While the footprint CHF accounts for the total heat dissipation, the wall CHF represents the effective heat flux on the channel wetted perimeter. As expected, CHF with geometry H was found to be higher compared to geometry C, especially in the low-mass-flux region. This is attributed to the slightly higher diameter of geometry H, where several correlations for CHF expect an increase with increasing equivalent diameter. On the other hand, the highest wall CHF is consistently obtained with geometry G. A possible explanation for the high CHF could be the result of the coupling effect of the enhanced heat transfer area of the corrugated walls and the continuous development of the liquid film layer that delays the dryout. The wall CHF and the corresponding critical (outlet) vapor quality with

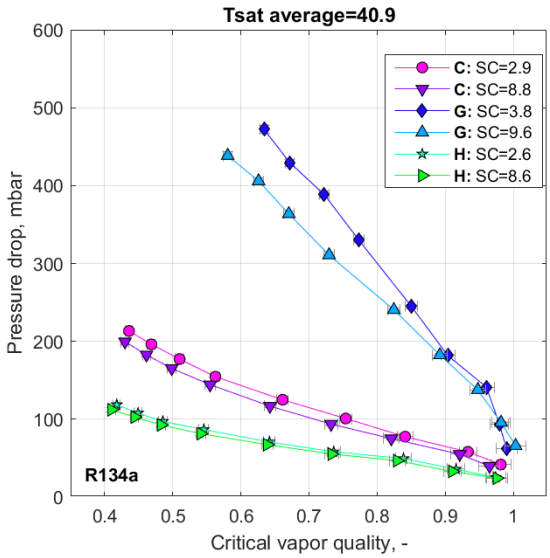

Fig. 8. Pressure drop vs. critical vapor quality for R134a at an average saturation temperature of 40.9 °C.

R134a at a saturation temperature of 40 °C is shown in Fig. 7b. The critical vapor quality represents the flow transition annular-to-dryout. It increases with higher wall CHF and the experimental points tend to collide into a single curve at very low wall CHF (low mass flux). In the case of geometry G, the vapor quality was found to be around 0.6 – 0.65 at the highest wall CHF, while for geometry H and C, it was around 0.35, meaning that the void fraction in geometry G was significantly higher. This result is suggested to be expressed by the higher wall heat fluxes obtained with geometry G, while the differences between geometry H and C could be explained by the different wetted diameter.

The pressure drop versus the vapor quality at saturation temperature of 40 °C with R134a is shown in Fig. 8. The pressure drop increases with decreasing vapor quality (heat flux increases) and it slightly reduces with inlet subcooling. As expected, the lowest pressure drop was found consistently with geometry H in all test conditions, while the highest pressure drop corresponded to geometry G.

3.3. Comparison with literature correlations

The comparison of 14 selected correlations for critical heat flux from literature with the experimental database of this investigation was performed. The correlations employed in the comparative analysis are developed for several channel types. Fig. 9 presents 4 of the 14 correlations compared with the measured CHF. The result of the comparison of the experimental results with the correlations is presented in Table 3. The table indicates the mean absolute error (MAE), ±20% and ±30% data point coverages, and important remarks on the channel type, heated equivalent diameter, and fluids used to develop the correlations. The best prediction method is obtained by Wu et al. with a coverage of 100% within the ±30% error band and MAE = 8.3%, and Kærn et al. [3]. With 92% coverage and MAE = 10.7%. In general, none of the remaining correlations can accurately predict the database from this investigation. This is especially true for the experimental data for the sinusoidal wavy test sample (geometry G) where most correlations underpredict the wall CHF. This is expected since all the selected correlations do not account for the enhanced area and delayed CHF achieved by corrugated channels.

4. Discussion

The maximum CHF achieved in the present investigation was 40% higher than in previous studies [3,5]. CHF increase is significant with corrugated wall channels, but it is moderate with diverging walls. The effect of mass flux on the CHF is confirmed, and the effect of inlet subcooling with geometry C and H was in accordance with previous studies [2,3]. However, the reverse trend found with geometry G appeared to be intrinsic to the corrugated walls, and a direct comparison with previous studies was difficult to make. Nonetheless, the IR thermal maps for geometry G indicated a uniform temperature distribution between the RTDs, even at the inlet section of the channels, while this was not the case for geometry H and C, where a temperature gradient of few degrees was evident. The very high heat fluxes coupled with the flow mixing in the wavy channels were found to be a reasonable conclusion for the negligible subcooling effect in the high-mass-flux region.

From the saturation temperature perspective, the reduction in the footprint CHF with increased saturation temperature in Fig. 5 is in accordance with the experimental results found by Kærn et al. [3]. Increasing the saturation temperature from 30 °C to 40 °C causes an increment in the vapor-to-liquid density ratio ρ_v/ρ_L (from 0.03 to 0.04) which stabilizes the flow by reducing the gap between the liquid and vapor phase, which in accordance with several correlations in the literature, expect an increase on the CHF with an increase of ρ_v/ρ_L. However, the decrease of the latent heat of vaporization h_{lv} (from 171.5 to 162.0 kJ/kg), and the surface tension reduction σ (from 7.1 to 6.0 mN m^{-1}) overcomes these effects resulting in a lower CHF. It is important to notice that a concrete conclusion cannot be made since the range of saturation temperature in the pres-

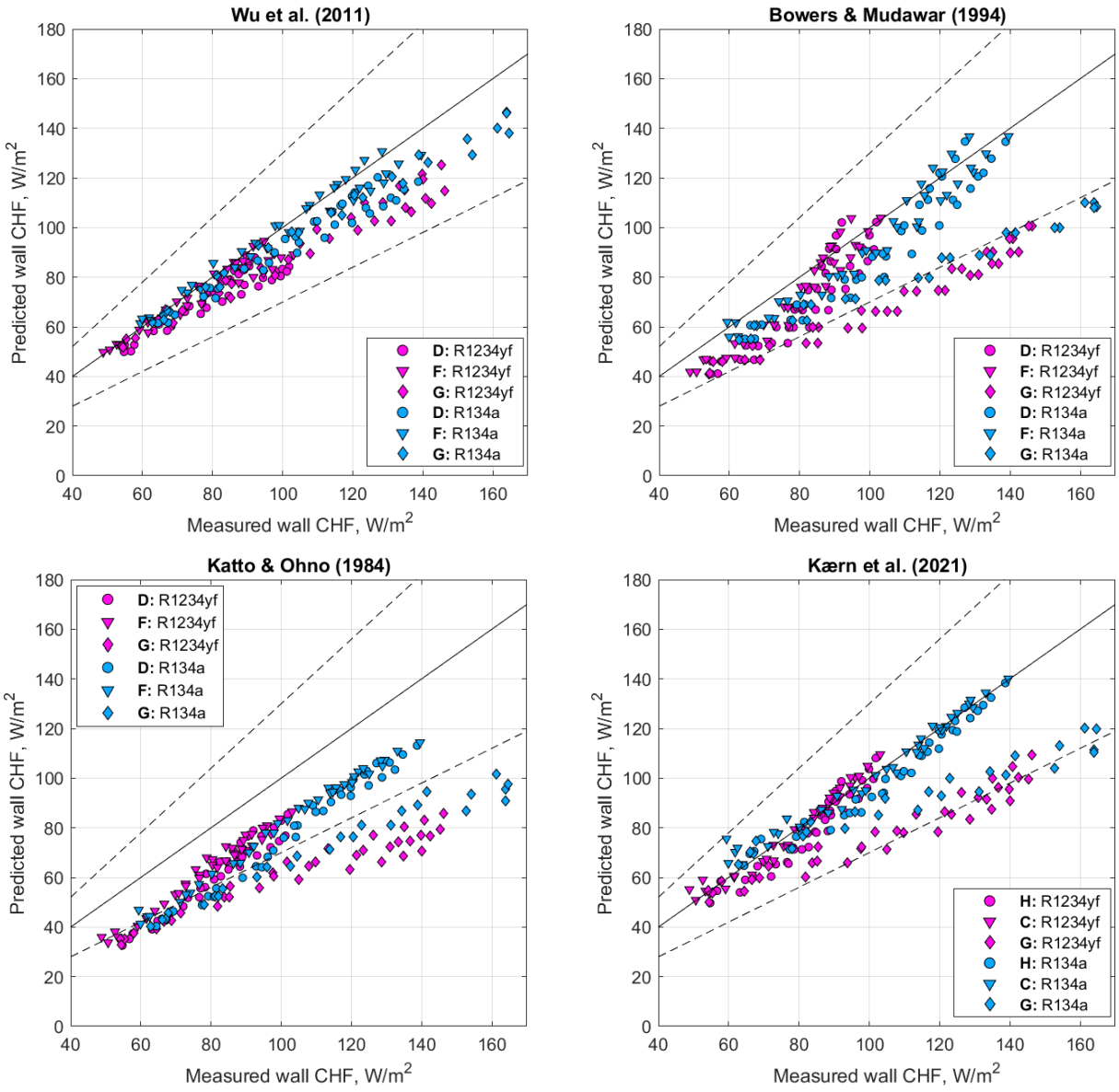

Fig. 9. Parity plot of four of the selected correlations for CHF and the measured CHF.

Table 3. Prediction statistics of four of the selected correlations.

Correlation	MAE [%]	**Coverage** [%]		**Remarks**:		
		±20%	±30%	Channel type	D_{he} [mm]	FLuids
Bowers and Mudawar	17.5	61.1	77.3	multi rectangular channels	2.54 – 0.51	R113
Wu et al.	8.3	97.2	100	general microchannels	0.22 – 2.98	water, refrigerants, nitrogen
Katto and Ohno	28.6	26.4	55.1	general conventional microchannels		water, refrigerants, nitrogen
Kærn	10.7	76.9	92.1	multi rectangular channels	0.36 – 0.52	R134a, R1234yf, R1234ze(E)

ent study was not wide, and Mauro and Thome's [2] suggestion of the existence of an optimal saturation temperature (peak in CHF) cannot be verified with the results obtained in this experimental investigation. The refrigerant R1234yf resulted in lower CHF compared to the traditional R134a. While the vapor-to-liquid density ratio ρ_v/ρ_L is 27% lower for R134a, the latent heat of vaporization h_{lv} is 18% higher compared to R1234yf at 30 °C saturation temperature. Consequently, it could be that the higher footprint CHF with R134a is mainly analogous to the difference in the latent heat of vaporization with the other fluid.

The wall CHF with geometry H was up to 15% higher compared to geometry C. This is aligned with the experimental results found by Fu et al. [4] with their diverging microchannels where the CHF increase was

higher, especially at low mass fluxes. The flow stability enhancement on the two-phase flow could partly explain the increase in the wall CHF. Nonetheless, the aspect ratio of the expanding channels could also affect the wall CHF increase. A previous study [4] demonstrated that the aspect ratio leads to the different behavior of the liquid film layer around the corners of the microchannels. Indeed, the aspect ratio at the exit of geometry H decreases which possibly leads to a thicker liquid layer. On the other hand, the pressure drop reduction with geometry H was attributed to the flow deceleration in the diverging channel.

Regarding the current prediction methods, Katto and Ohno's correlation is one of the most widely quoted among other authors, and their prediction was relatively well aligned with the results but underpredicting overall, resulting in MAE = 28.6%. In a recent study, Kærn et al. [3] proposed a modified Katto and Ohno correlation to account for the subcooling effect. In fact, the correlation proposed by Kærn et al. provides one of the best predictions with MAE = 10.7%. This is not surprising since the correlation was specifically developed with a database from the same laboratory. Wu et al. correlation gave the best prediction. Their regression employed their results from water, and Bower and Mudawar data in R-113, alleging the drastic fluid property differences and different geometry made their correlation suitable for multiple cases. However, the calculation of the wall heat flux q_w used in their regression did not consider the fin efficiency, thus, ignoring the conduction effect and assuming the fin has a uniform temperature in its entire length which is not true. Coincidentally, even if the correlation by Wu et al. accurately predicts the data with MAE = 8.9%, it is important to indicate the different data regression of the wall CHF employed by the authors and the unaccounted subcooling effect.

5. Conclusion

The CHF is an important issue during flow boiling in power electronics, and accurate CHF prediction requires a well-founded understanding of the CHF mechanism and the effect of its main parameters. In general, with both working fluids, the main observations found were the following:

- When G increases, CHF increases.
- When D increases, CHF increases.
- When $\Delta \mathrm{T}_{\mathrm{sc}}$ increases, CHF increases with straight and diverging channels, but it is unaffected with wavy sinusoidal channels.
- When $\mathrm{T}_{\mathrm{sat}}$ increases, CHF decreases.
- Wavy geometry enhances CHF.
- Diverging channels decrease the pressure drop.

The results of the investigation introduce several features in which further and deeper analysis is required to consolidate comprehensive characterizations of the effects of main parameters of interest on CHF. Multi-channel setups with alternative sidewall geometry present a variety of phenomena that are difficult to segregate in experiments. Therefore, detailed numerical models could be coupled to the description of the CHF mechanism in alternative geometries. On the other hand, only a patient collection of experimental data for the step-by-step creation of an extensive database of measured CHF could effectively improve the prediction of future correlations.

Acknowledgments

The present investigation was jointly supported by the Thermal Section in the Mechanical Department of the Technical University of Denmark.

References

[1] J. Lee, I. Mudawar, Critical heat flux for subcooled flow boiling in microchannel heat sinks, Int. J. Heat Mass Transf. 52 (2009) 3341–3352.doi: 10.1016/j.ijheatmasstransfer.2008.12.019.

[2] Mauro, A., Thome, J., Toto, D., & Vanoli, G. (2010). Saturated critical heat flux in a multi-microchannel heat sink fed by a split flow system. Experimental Thermal and Fluid Science, 34(1), 81--92.doi: https://doi.org/10.1016/j.expthermflusci.2009.09.005

[3] Kærn, M., Criscuolo, G., Meyer, K., & Markussen, W. (2021). Critical heat flux characteristics of R1234yf, R1234ze (E), and R134a during saturated flow boiling in narrow high aspect ratio microchannels. International Journal of Heat and Mass Transfer, 180, 121840.doi: https://doi.org/10.1016/j.ijheatmasstransfer.2021.121840

[4] Fu, B., Lee, C., & Pan, C. (2013). The effect of aspect ratio on flow boiling heat transfer of HFE-7100 in a microchannel heat sink. International journal of heat and mass transfer, 58(1-2).doi: https://doi.org/10.1016/j.ijheatmasstransfer.2012.11.050

[5] Xia, G., Tang, Y., Zong, L., Ma, D., Jia, Y., & Rong, R. (2019). Experimental investigation of flow boiling characteristics in microchannels with the sinusoidal wavy sidewall. International Communications in Heat and Mass Transfer, 101, 89--102.doi: https://doi.org/10.1016/j.icheatmasstransfer.2019.01.006

[6] Park, J., & Thome, J. (2010). Critical heat flux in multi-microchannel copper elements with low pressure refrigerants. International Journal of Heat and Mass Transfer, 53(1-3), 110--122.doi: https://doi.org/10.1016/j.ijheatmasstransfer.2009.09.047

[7] Describing uncertainties in single-sample experiments. (1953). ASME Mechanical Engineering, 75(1), 38. doi: ISSN 19435649, 00256501